International Journal of Technology (2016) 8: 1344-1351
ISSN 2086-9614

COMPUTATIONAL FLUID DYNAMIC APPLICATION IN SCALE-UP OF A STIRRED-BATCH REACTOR FOR DEGUMMING CRUDE PALM OIL

Yuswan Muharam[1*], Aditya Kurniawan[1]

[1]*Department of Chemical Engineering, Faculty of Engineering, Universitas Indonesia, Kampus UI Depok, Depok 16424, Indonesia*

(Received: November 2016 / Revised: December 2016 / Accepted: December 2016)

ABSTRACT

The research aims to scale up a small-scale stirred batch reactor to a large-scale stirred batch reactor in order to degum crude palm oil for use as a raw material in biodiesel production. The scale-up is based on the similarity of fluid Reynolds numbers in the two differently sized reactors. To achieve this aim, computational fluid dynamic modeling and simulations of the two reactors were performed. A small-scale palm oil degumming process was carried out in a 250 cc autoclave reactor using a magnetic stirrer at 500 rpm. The simulation results of this small reactor yielded a fluid Reynolds number in the range of 5 to 3,482. The large-scale reactor proposed in this research is 1.25 m^3 in volume and is equipped with two impellers: a pitched blade impeller and a Rushton turbine impeller. The pitched blade impeller is placed over the Rushton turbine impeller. They are rotated at 100 rpm. Under this setting and operation, the resulting fluid Reynolds number was in the range of 486 to 202,000. This result indicates that the large-scale reactor was able to reproduce the reaction performance obtained in the small-scale reactor.

Keywords: Batch reactor; Biodiesel; Computational fluid dynamics; Degumming; Scale up

1. INTRODUCTION

Biodiesel is used as an alternative fuel in standard diesel engines. It can be used alone or blended with petrodiesel in any proportion (Omidvarborna et al., 2014). In order to boost the utilization of biofuel, the Ministry of Energy and Mineral Resources of the Republic of Indonesia ratified Regulation No.12/2015 with the minimum obligation of using biodiesel as a blended fuel. In micro businesses, fishery businesses, agricultural businesses, transportation, industry and commerce, the minimum content of biodiesel is 20% and 30% for power generation (Sugiyono et al., 2015).

Similar to other fats and oils, crude palm oil (CPO) contains phospholipids, which are also called gums. Phospholipids must be removed because they have emulsifying properties. If they are not removed, they may lead to failure in the phase separation during the transesterification process, which inhibits the emulsion-breakdown process. Consequently, the biodiesel yield decreases (Kim et al., 2002; Kekre, 2007). Phospholipids are usually removed by hydration with water, phosphoric acid, and polybasic organic acids, either individually or in combination. The gum removal process is referred to as degumming. The treatment with phosphoric acid (H_3PO_4) involves the mass transfer of gum molecules in the CPO phase, the mass transfer of gum molecules through the CPO–H_3PO_4 interface, the mass transfer of gum molecules in

*Corresponding author's email: muharam@che.ui.ac.id, Tel. +62-21-7863516, Fax. +62-21-7863516
Permalink/DOI: https://doi.org/10.14716/ijtech.v7i8.6898

H_3PO_4 phase, and the reaction between the gum molecules and the H_3PO_4 molecules in the H_3PO_4 phase. The reaction produces a greater number of hydratable gums.

The previous research on degumming kinetics was conducted to eliminate other elements in the process, except interface mass transfer and chemical reaction, with the aim of developing an intrinsic kinetic model by thoroughly mixing the fluid in small-scale reactors. Hence, mixing efficiency was achieved and interface mass transfer and chemical reaction were the only rate-limiting steps (Ristianingsih et al., 2011). However, thorough mixing in large-scale reactors is difficult, which reduces mixing efficiency.

In order to ensure that the performance of small-scale reactors is preserved when the volume of the process is enlarged, the scale-up process is performed. However, the scale-up is not always easy because the optimal conditions in small-scale reactors are often not optimal in large-scale reactors (Post, 2010). In the scale-up process, the relationship nD^x = constant can be used if there is geometrical similarity (Paul et al., 2003).

The present study investigates a problem that occurs in scaling up the degumming process, which is caused by the different geometries of small-scale and large-scale reactors. The different geometries lead to different flow patterns and velocity distributions. In this work, therefore, computational fluid dynamics (CFD) is used to simulate the flow in the differently scaled reactors used for degumming. The criteria parameters are compared to obtain a mixing capability that is similar in both small-scale and large-scale reactors.

2. EXPERIMENTAL METHOD

The kinetics of degumming was investigated by Ristianingsih et al. (2011) in an autoclave using phosphoric acid (H_3PO_4). The H_3PO_4 solution (80% concentration) was a 1.5% volume of CPO. The maximum conversion was obtained at 80°C and a mixing speed of 500 rpm. The decrease in the gum content was almost 50% of the initial content. These parameters were used in a simulation to estimate the flow in the small-scale vessel.

Even though the CPO and H_3PO_4 phases are immiscible, because of the low volume fraction of the dispersed phase (H_3PO_4), the system may be regarded as a dilute solution when the dispersion is only affected by the hydrodynamics of the continuous phase (CPO). In contrast, the flow field of the continuous phase is not affected by the dynamics of dispersed phase, including drop coalescence and deformation (Paul et al., 2003; Albright, 2008). Therefore, the flow of the continuous phase is modeled using the Rotating Machinery-Turbulent Flow module available in COMSOL.

The scale-up of a small-scale reactor to a large-scale reactor was performed by modeling both reactors, and then using the models to conduct a simulation to obtain the mixing parameters of flow patterns, velocity distributions, and fluid Reynolds numbers. Finally, the parameters of the small-scale and large-scale reactors are compared to determine their similarity.

3. MODELING

3.1. Transport Equation

In order to simulate flow at high Reynolds numbers in geometries with one or more rotating parts, COMSOL provided the Rotating Machinery-Turbulent Flow module. The momentum balance is governed by the Navier-Stokes equation as follows:

$$\rho \frac{\partial \mathbf{u}}{\partial t} + \rho(\mathbf{u}.\nabla)\mathbf{u} = \nabla.[-p\mathbf{I} + (\mu + \mu_T)(\nabla\mathbf{u} + (\nabla\mathbf{u})^T)] + F \quad (1)$$

where **u** denotes the velocity of the continuous phase, ρ is the density of the continuous phase, p is the pressure, μ is the viscosity of fluid, μ_T is the turbulent/eddy viscosity as the additional inertial effect caused by turbulence, and F is the additional force.

The mass conservation is governed by the continuity equation:

$$\rho \nabla . \mathbf{u} = \mathbf{0} \tag{2}$$

The turbulence effect is modeled using the k-ε model. The model introduces two additional transport equations and two dependent variables: turbulence kinetic energy (k) and turbulence dissipation rate (ε). The balances of both are described by Equation 3 and Equation 4, respectively:

$$\rho \frac{\partial k}{\partial t} + \rho(\mathbf{u}.\nabla)k = \nabla.\left[\left(\mu + \frac{\mu_T}{\sigma_k}\right)\nabla k\right] + P_k - \rho\varepsilon \tag{3}$$

$$\rho \frac{\partial \varepsilon}{\partial t} + \rho(\mathbf{u}.\nabla)\varepsilon = \nabla.\left[\left(\mu + \frac{\mu_T}{\sigma_\varepsilon}\right)\nabla \varepsilon\right] + C_{\varepsilon 1}\frac{\varepsilon}{k}P_k - C_{\varepsilon 2}\rho\frac{\varepsilon^2}{k} \tag{4}$$

Turbulence viscosity emerging in the Navier-Stokes equation is modeled as follows:

$$\mu_T = \rho C_\mu \frac{k^2}{\varepsilon} \tag{5}$$

The turbulence model constants emerging in those equations are as follows: C_μ = 0.09, $C_{\varepsilon 1}$ = 1.44, $C_{\varepsilon 2}$ = 1.92, σ_k = 1.0, and σ_ε = 1.3. The production term, P_k is defined as

$$P_k = \mu_T[\nabla \mathbf{u} : (\nabla \mathbf{u} + (\nabla \mathbf{u})^{\boldsymbol{T}})] \tag{6}$$

The rotational frequency, direction, and the axis of rotation are defined in a rotating domain.

3.2. Boundary Conditions

In the Navier-Stokes turbulent equation, the flow of fluid contacting a solid wall is expressed by the wall function:

$$\mathbf{u}.\mathbf{n} = 0 \tag{7}$$

Shear stress on the wall is described by

$$[(\mu + \mu_T)(\nabla \mathbf{u} + (\nabla \mathbf{u})^T)]\mathbf{n} = -\rho\frac{u_\tau}{\delta_w^+}u_{tang}\,;\; u_{tang} = \mathbf{u} - (\mathbf{u}.\mathbf{n})\mathbf{n} \tag{8}$$

Turbulent kinetic energy and turbulent dissipation on the wall are defined by

$$\nabla k.\mathbf{n} = \mathbf{0};\; \boldsymbol{\varepsilon} = \boldsymbol{\rho}\frac{C_\mu k^2}{\boldsymbol{\kappa_V}\delta_w^+\mu} \tag{9}$$

3.3. Small-scale Geometry

The small-scale reactor modeled in the present study is the autoclave reactor used in previous degumming kinetic studies (Ristianingsih et al., 2011), which has a diameter of 7.816 cm (D_{fluid}). Only the part of the reactor volume that contains reaction fluid is modeled at a height of

3.416 cm (H_{fluid}). This gives the fluid volume of 250 cc, as shown in Figure 1. The reactor is equipped with a stirrer bar 3.175 cm in length and 0.9525 cm (3/8 inch) in diameter. The stirrer bar is rotated with the rotational frequency of 500 rpm.

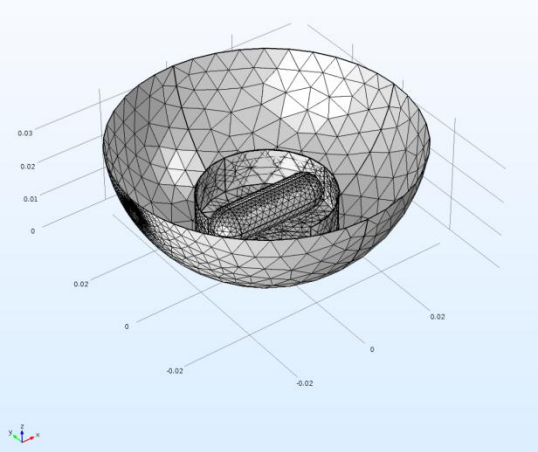

Figure 1 Small-scale reactor model

3.4. Large-scale Geometry

The large-scale geometry is a vessel with dish bottom equipped with two-stage impellers, as shown in Figure 2. The upper stage is an axial type impeller (pitch blade), and the lower stage is a radial type impeller (Rushton turbine).

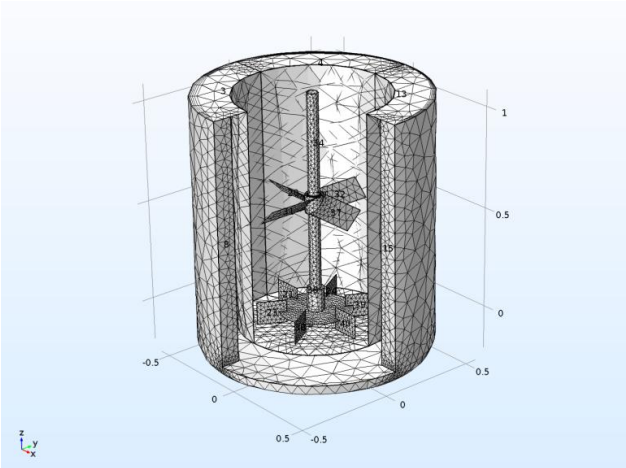

Figure 2 Large-scale reactor model

The diameter of the active fluid D_{fluid} is 1.124 m, and the fluid height H_{fluid} is 1.289 m, which gives a fluid volume of 1.25 m^3. The capacity is sufficient to produce 4 tons of biodiesel per batch through homogeneous-based catalyzed transesterification. The diameter of both the axial and radial impellers is 0.562 m. The clearance between the lower impeller and the vessel bottom is 0.12 m, and the spacing between the two impellers is 0.54 m or half of the shaft length. The vessel is baffled on four sides (spacing at 90^o). The width of the baffle is 0.094 m or 1/12 of the vessel diameter. The rotational frequency of both impellers is 100 rpm.

3.5. Similarity Criteria

In scaling up mixing, many similar parameters may be used to reproduce a small-scale performance as are used to produce a large-scale performance. In scaling up based on the CFD concept, hydrodynamic parameters, such as the fluid Reynolds number, are used as similar

parameters. Therefore, fluid Reynolds number and velocity are used as the similarity parameters in this research. The fluid Reynolds number Re_{fluid} is formulated as follows:

$$Re_{fluid} = \frac{\rho v D_{reactor}}{\mu} \quad (10)$$

where $D_{reactor}$ is the diameter of the reactor.

4. SIMULATION

4.1. Velocity Distribution

The average flow pattern and velocity magnitude of the spatial domain were obtained by running the model in stationary mode (frozen rotor). The simulation results for the flow pattern, the velocity distribution and the fluid Reynolds number in the small-scale reactor are shown in Figure 3 and Figure 4, respectively.

Figure 3 shows that a vortex is formed in the reactor. The flow circulates around the axis because the tube is un-baffled. The mixing occurs predominantly in the radial direction as indicated by the red arrow. At the top, the flow rotates from the axis center outward and slightly downward before rotating regularly near the stirrer bar.

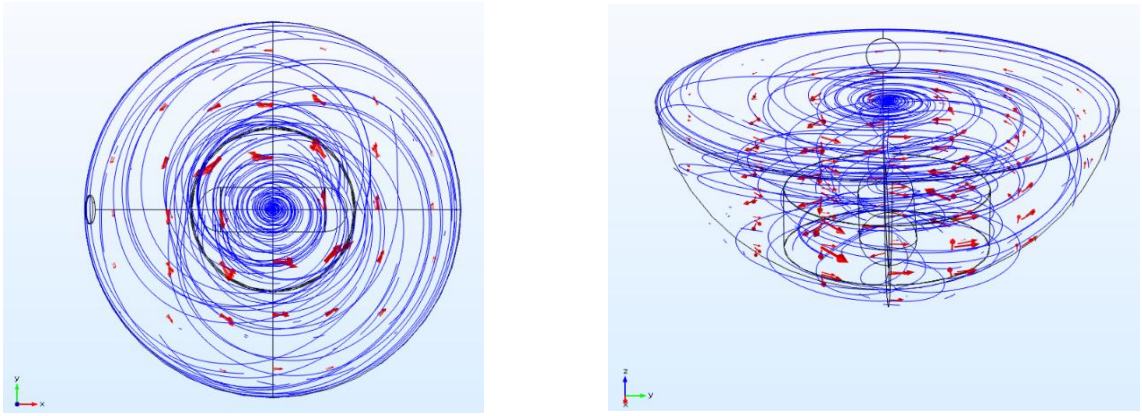

(a) (b)

Figure 3 Flow pattern in the small-scale reactor: (a) top view; and (b) side view

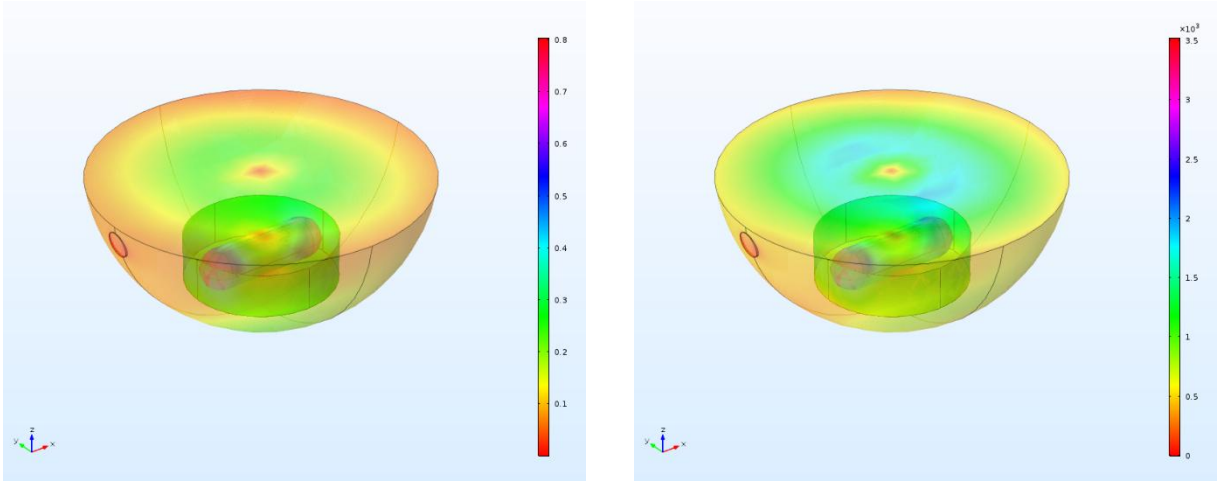

(a) (b)

Figure 4 The distribution of: (a) velocity; and (b) fluid Reynolds number in the small-scale reactor

Figure 4 shows that the maximum velocity occurs in the fluid elements in contact with the tip of the stirrer bar. The velocity reduces in the radial direction as indicated by the color legend. The fluid velocity around the axis above the stirrer is very small because the flow pattern around the axis is vertical and spiral-shaped, as shown in Figure 3. From the axis radially outward, the velocity increases and then decreases to the reactor wall. The same trend occurs in the fluid Reynolds number, which increases radially outward until the fluid is closer to the reactor wall than to the increase in velocity.

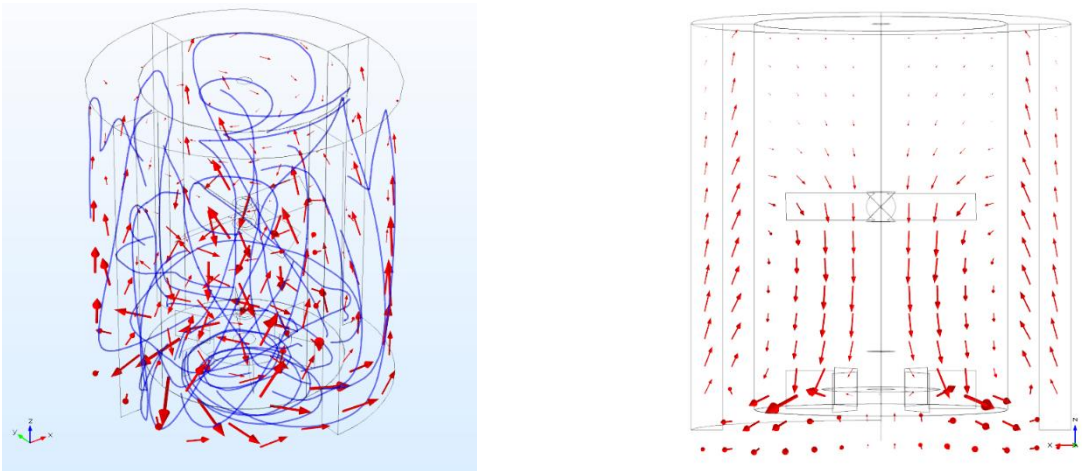

(a) (b)

Figure 5 Flow pattern in the large-scale reactor: (a) 3D; and (b) side view

The simulation results of the large-scale reactor are depicted in Figure 5, Figure 6, and Figure 7. As Figure 5 shows, the flow pattern in the large-scale reactor is highly different from that in the small-scale reactor. The fluid flows radially outward because of the rotation of the lower impeller, and it flows in the axial direction because of the rotation of the upper impeller. Four baffles on the reactor wall serve to direct the flow axially upwards so that the vortex created by the rotation of the lower impeller is irregularly shaped. The flow is then redirected downward by the upper impeller in the middle of the reactor. Overall, the flow pattern is irregular, which is caused by the combination of the radial flow and the axial flow.

Figure 6a and Figure 7a show that the maximum velocity occurs in the fluid that is in contact with the lower impeller. The velocity decreases from the lower impeller radially outwards and then increases again near the baffles. The reason is that the radial flow near the baffles is generated by the lower impeller. It knocks against the baffles, and it then is diverted to form the axial flow to the top of the vessel. This is called the wall jet effect, which distributes the velocity inside the reactor.

The velocity around the upper impeller exhibits the same trend as the lower impeller but with a smaller velocity gradient (Figure 6b). The reason is that the flow arriving from the bottom is directed to the center and then knocked by the upper impeller to flow downward (Figure 5b).

The distribution of the fluid Reynolds number resembles that of the velocity, as shown in Figure 7b. The maximum fluid Reynolds number occurs in the fluid that is in contact with the lower impeller. The fluid Reynolds number decreases from the lower impeller radially outwards and then increases again near the baffles. The same trend in the fluid Reynolds number occurs in the upper part of the reactor.

The frequencies of the velocity and the fluid Reynolds numbers in the small-scale reactor and the large-scale reactor are shown in Figure 8. Figure 8a shows that the highest possible velocity

in the small-scale reactor is 0.08 m/s. In the large-scale reactor, no particular velocity is predominant. More than 99% of the fluid in the large-scale reactor has a velocity greater than 0.08 m/s.

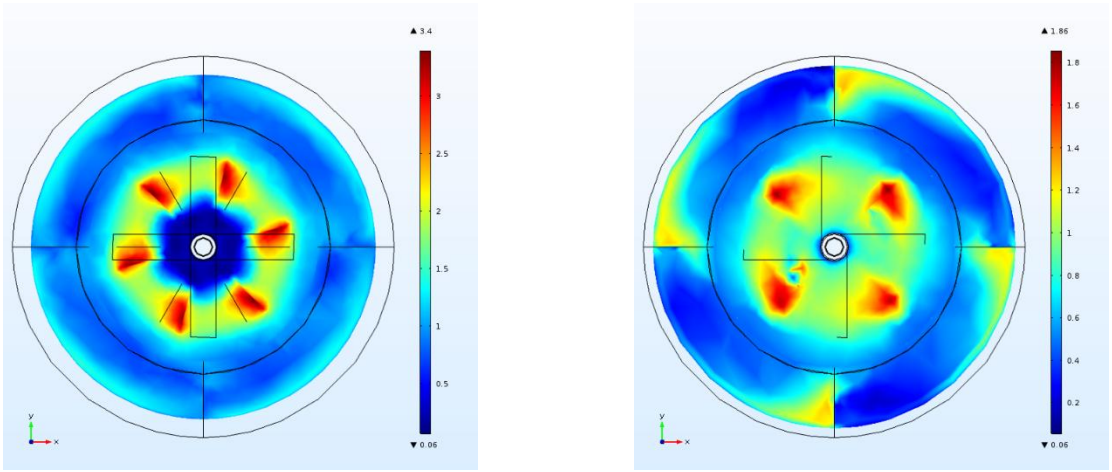

(a) (b)

Figure 6 Velocity distribution around (a) the lower impeller and (b) the upper impeller

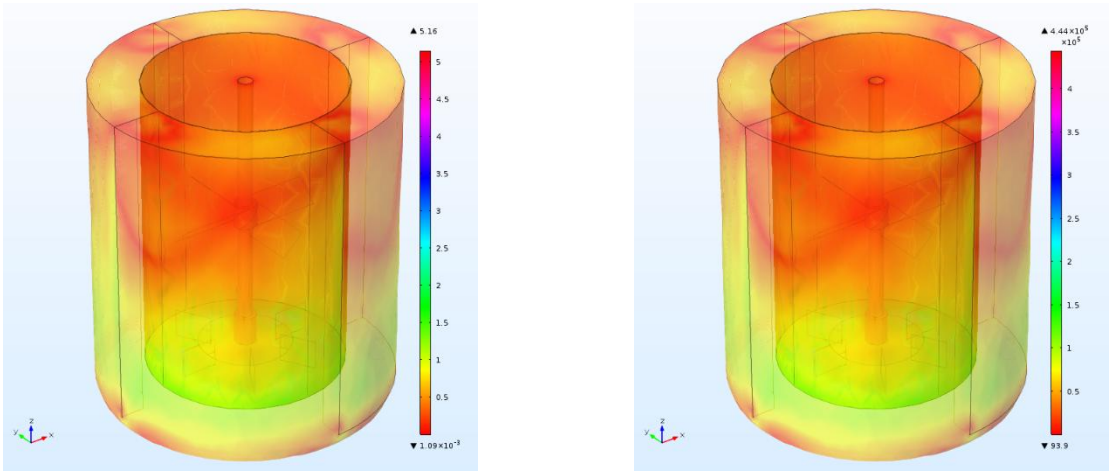

(a) (b)

Figure 7 Distribution of: (a) velocity; and (b) fluid Reynolds number in the large-scale reactor

As shown in Figure 8b, the fluid Reynolds numbers in the small-scale reactor and the large-scale reactor are within the range of 5 to 3,482 and 486 to 202,000, respectively. The most frequent Reynolds number in the small-scale reactor is 480. In the large-scale reactor, two fluid Reynolds numbers are the most frequent, i.e., 77,800 and 88,000. More than 99% of the fluid in the large-scale reactor possesses a fluid Reynolds number larger than that in the small-scale reactor.

The velocity and fluid Reynolds number relate to the mixing characteristics and mass transfer limitations in the continuous and dispersed phases and in the interface. As observed by Ristianingsih et al. (2011), the mixing in the small-scale reactor was considered to have succeeded in eliminating the mass transfer limitations, except the interface. Therefore, under the steady-state condition in this study, the comparison of the velocities and the fluid Reynolds numbers of the two scales of the reactor, the results showed that the large-scale reactor fulfilled the mixing criteria of the small-scale reactor and reproduced the reaction performance that was obtained in the small-scale reactor.

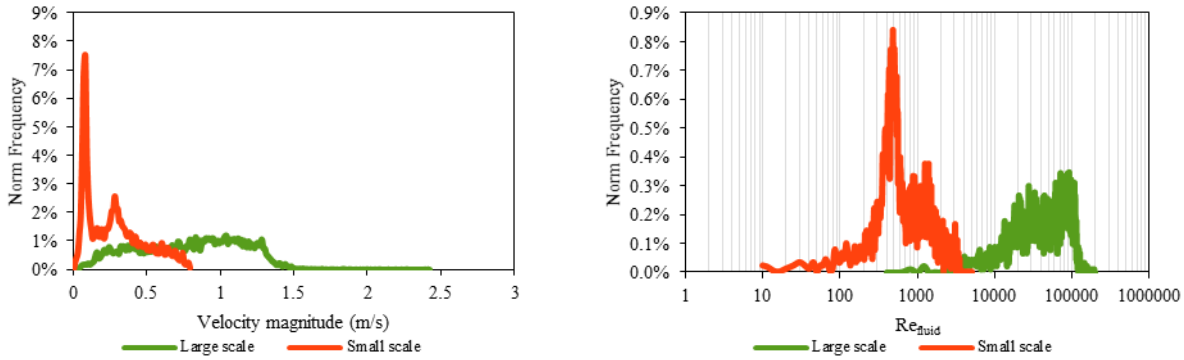

(a) (b)

Figure 8 Frequency of: (a) velocity; and (b) fluid Reynold number

5. CONCLUSION

This study increased the size of a stirred batch reactor from a small scale to a large scale for the degumming of crude palm oil to use as the raw material in biodiesel production. In comparing the velocities and the fluid Reynolds numbers of the two scales of the reactor, the results showed that the large-scale reactor fulfilled the mixing criteria of the small-scale reactor and reproduced the reaction performance that was obtained in the small-scale reactor. Subsequent research will focus on improving the model by considering its use in multiphase mixing.

6. ACKNOWLEDGEMENT

We express our gratitude to the University of Indonesia, which funded this research through the scheme of Indexed International Publication Grant for Final Project (*Hibah Publikasi Internasional Terindeks untuk Tugas Akhir*) No. 2099/UN2.R12/HKP.05.00/2016.

7. REFERENCES

Albright, L., 2008. *Albright's Chemical Engineering Handbook*, Taylor & Francis

Kekre, N., 2007. *Investigation of Phospholipid Separation from Soybean Oil for Biodiesel Production*. Retrospective Theses and Dissertations, Iowa State University, 63

Kim, I.C., Kim, J.H., Lee, K.H., Tak, T.M., 2002. Phospholipids Separation (Degumming) from Crude Vegetable Oil by Polyimide Ultrafiltration Membrane. *Journal of Membrane Science*, Volume 205, pp. 113–123

Omidvarborna, H., Kumara, A., Kim, D.S., 2014. Characterization of Particulate Matter Emitted from Transit Buses Fueled with B20 in Idle Modes. *Journal of Environmental Chemical Engineering*, Volume 2(4), pp. 2335–2342

Paul, L.P., Victor, A.A-O., Suzanne, M.K., 2003. *Handbook of Industrial Mixing: Science and Practice*, Wiley, Hoboken, NJ

Post, T., 2010. *Understand the Real Worlds of Mixing*. CEP, March, pp. 25–32

Ristianingsih, Y., Sutijan, Budiman, A., 2011. Kinetics Study of Chemical and Physical Process of Gum Removal from Crude Palm Oil (CPO) using Phosphoric Acid. *Reaktor*, Volume 13(4), pp. 242–257

Sugiyono, A., Anindhita, Boedoyo, M.S., Adiarso, 2015. *Indonesian Energy Outlook 2015, Centre for Energy Resources Development Technology and Agency for the Assessment and Application of Technology*, BPPT